Synthesis, Properties, and Theoretical Characterization of Largely π-Extended Tetrathiafulvalene Derivatives with Quinonoid Structures

Nazario Martín,* Luis Sánchez, and Carlos Seoane

Departamento de Química Orgánica, Facultad de Química, Universidad Complutense, E-28040 Madrid, Spain

Enrique Ortí,* Pedro M. Viruela, and Rafael Viruela

Departamento de Química Física, Universidad de Valencia, E-46100 Burjassot (Valencia), Spain

Received October 21, 1997

A series of highly conjugated tetrathiafulvalene (TTF) analogues with a quinonoid structure has been synthesized, and their structural and electronic properties have been characterized by both experimental techniques and quantum-chemical calculations. Cyclic voltammetry measurements show a two-electron oxidation wave to form the dication, which is mainly located on the dithiole rings. The second irreversible oxidation wave to form the trication-radical corresponds to the oxidation of the polyacenic backbone. The temperature dependence of the reduction peak corresponding to the donor^{2+} → donor^{0} process is explained in terms of the low stability of the cation and the high aromaticity of the dication. Charge-transfer complexes are formed with the strong acceptor $TCNQF_4$ showing a 1:2 (D:A) stoichiometry and a semiconducting behavior. The molecular structures of neutral and oxidized compounds are investigated by performing theoretical calculations at the semiempirical, ab initio, and density functional theory levels. The steric hindrance introduced by lateral benzoannulation determines the loss of planarity of the neutral molecules, which adopt butterfly shaped structures. The folded structures are retained in the cations, reducing the gain of aromaticity in the first oxidation step. The dications are by contrast predicted to be fully aromatic and are formed by a planar polyacenic moiety and two orthogonal, singly charged dithiole rings. The destabilization of the cations and the high aromaticity of the dications explain the redox properties observed experimentally. Theoretical calculations also help to rationalize the UV−vis data since they predict the appearance of a low-energy charge-transfer absorption band for the neutral compounds where the laterally fused polyacenic units act as acceptors.

Introduction

During the past few years, a considerable research effort has been focused upon the synthesis of more sophisticated tetrathiafulvalenes.[1] In this regard, the preparation of extended π-donors in which the two dithiole rings are separated by a conjugated spacer have recently received particular attention as a consequence of their potential interest in the preparation of materials with increased dimensionality,[2] nonlinear optical properties,[3] or as small-gap semiconductors.[4] Donor systems with extended π-conjugation additionally present a lowering of the oxidation potential due to charge delocalization and a decrease of the Coulombic repulsion in the dication state. This is important in the strategy for the molecular design of novel donor π-systems.[1,5]

Examples of structural modifications on extended π-donors in which the two dithiole units of the tetrathiafulvalene (TTF) molecule (**1a**) are separated by different conjugated spacer groups are shown in Chart 1. Vinylogues of TTF of type **2** were first reported by Yoshida et al.[6] (**2a**) and, later, the analogous BEDT−TTF (**2b**) was prepared by following a more general synthetic route.[7] These compounds (**2a**, **2b**) show stronger donor properties than the parent TTF (**1a**) or BEDT−TTF (**1b**) and present a smaller difference between the first and second oxidation potentials.

The same electrochemical behavior is observed for compounds **3**. These elongated donors containing an heterocyclic spacer were recently prepared, and highly conducting molecular complexes with acceptor molecules have been derived from them.[8] Compounds **4a**−**c** also show two single-electron reversible oxidation waves and result to be good candidates for the preparation of organic

(1) Khodorkovsky, V.; Becker, J. V. In *Organic Conductors: Fundamentals and Applications*; Farges, J. P., Ed.; Marcel Dekker: New York, 1994; Chapter 3, p 75.

(2) Bryce, M. R. *J. Mater. Chem.* **1995**, *5*, 1481 and references therein.

(3) Jen, A. K.; Rao, V. P.; Drost, K. J.; Wong, K. Y.; Cava, M. P. *J. Chem. Soc., Chem. Commun.* **1994**, 2057.

(4) Brisset, H.; Thobie-Gautier, C.; Jubault, M.; Gorgues, A.; Roncali, J. *J. Chem. Soc., Chem. Commun.* **1994**, 1765.

(5) Takahashi, K.; Tomitani, K.; Ise, T.; Shirahata, T. *Chem. Lett.* **1995**, 619.

(6) Yoshida, Z.; Kawase, T.; Awaji, H.; Sugimoto, I.; Sugimoto, T.; Yoneda, S. *Tetrahedron Lett.* **1983**, *24*, 3469. Awaji, H.; Sugimoto, T.; Misaki, Y.; Kawase, T.; Yoneda, S.; Yoshida, Z. *Chem. Mater.* **1989**, *1*, 535.

(7) Khodorkovskii, V. Y.; Veselova, L. N.; Neilands, O. Y. *Khim. Geterotsikl. Soedin.* **1990**, 130; *Chem Abstr.* **1990**, *113*, 22868t. Hansen, T. K.; Lakshmikantham, M. V.; Cava, M. P.; Metzger, R. M.; Becher, J. *J. Org. Chem.* **1991**, *56*, 2720. Moore, A. J.; Bryce, M. R.; Ando, D.; Hursthouse, M. B. *J. Chem. Soc., Chem. Commun.* **1991**, 320. See also ref 2.

(8) Takahashi, K.; Tomitani, K. *J. Chem. Soc., Chem. Commun.* **1991**, 821. Takahashi, K.; Nihira, T.; Tomitani, K.; *J. Chem. Soc., Chem. Commun.* **1993**, 1617.

S0022-3263(97)01941-5 CCC: $15.00
Published on Web 02/03/1998

Chart 1. Some Representative Examples of π-extended TTF Derivatives

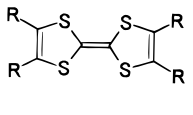

1a TTF (R= H)

1b BEDT-TTF (R,R= $(SCH_2)_2$)

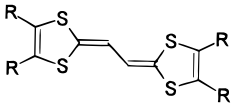

2a R= H

2b R,R= $(SCH_2)_2$

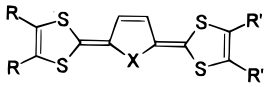

3a X= S

3b X= Se

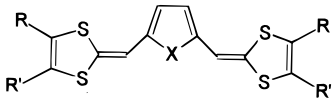

4a: X= O

4b: X= S

4c: X= Se

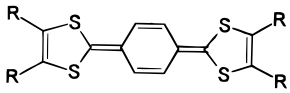

5a: R= H

5b: R, R= $(CH{=}CH)_2$

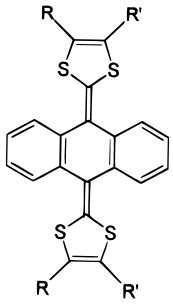

6a: R= R'= H

6b: R= R'= Me

6c: R= SMe; R'= Me

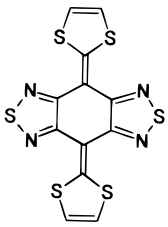

7

metals.[9,10] The influence of the heterocyclic spacer on the redox properties has been studied by using MNDO-PM3 calculations.[10]

p-Quinodimethane analogues of TTF such as **5**−**7** show very attracting properties due to their particular electronic and geometrical features. Compound **5a** is an extremely strong electron donor showing a very small difference between the first two oxidation potentials ($E^1_{1/2} = -0.11$; $E^2_{1/2} = -0.04$ V).[11] Compounds **6** exhibit, oppositely to all the aforementioned donors, a first quasireversible oxidation wave involving two electrons to form the dication. The first oxidation potential values, determined by cyclic voltammetry, are similar to that of the parent TTF, and highly conducting CT-complexes of **6b** with tetracyano-*p*-quinodimethane (TCNQ) showing a 1:4 stoichiometry have been described.[12] Compound **6c** has been reported to form a CT-complex with TCNQ leading to two types of black crystals.[13] The X-ray diffraction of one of these crystals proved to be a rather unusual complex, constituted by four different types of molecules: TCNQ, **6c**, H_2O, and two other molecules resulting from the oxidation of TCNQ by substitution of one cyano group by an oxygen atom in the TCNQ molecule.[13,14] In contrast to the **6b**·TCNQ complex, the complexes formed by **6c** and TCNQ did not show conducting properties.[15]

More recently, we have reported the synthesis and properties of the first dimeric donors derived from TTF with *p*-quinodimethane structures formed by two units of **6** connected through an oxygen atom.[16] The CV data indicated that these dimers behave electrochemically as two independent monomers, exhibiting a first oxidation wave involving a four-electron overall process.

The presence of one or two thiadiazole rings fused to the central quinonoid ring as in **7** does not destroy the planar geometry of the system, and **7** has a better electron−donating ability than the benzene-fused analogues **6**. Compound **7**, however, exhibits an extremely low solubility, which prevents the formation of conducting CT-complexes, although it has an unusually high conductivity as a single component conductor.[17]

The design of novel donor and acceptor molecules leading to an increase of dimensionality in the solid-state remains a major goal in materials science, and in this regard, extended π-electron donors deserve a deeper study.[2] However, despite the interest of these molecules in the preparation of novel organic conducting materials, π-extended donors constituted by polyacenic unit larger than the anthraquinodimethane system present in **6** have not been systematically studied.

In a previous paper,[18] we reported the synthesis and electrochemistry of the unsubstituted π-extended *p*-quinodimethane analogues of TTF 5,12-bis(1,3-dithiol-2-ylidene)-5,12-dihydronaphthacene (**13a**), 6,13-bis(1,3-dithiol-2-ylidene)-6,13-dihydropentacene (**14a**), and 5,14-bis(1,3-dithiol-2-ylidene)-5,14-dihydropentacene (**15a**). The mass spectrometric behavior of these donors has also been studied by exact mass measurements and metastable ion analysis and the influence on the fragmentation of the central linkage discussed.[19]

Taking into account that the presence of sulfur atoms on the periphery of the molecule is an efficient crystal engineering method for obtaining intermolecular interactions in TTF-based conducting materials, we now report a detailed study of the synthesis, electrochemical and spectroscopic characterization, and charge-transfer complexes preparation of new largely π-extended TTF derivatives with quinonoid structures and sulfur-containing

(9) Benhamed-Gasmi, A. S.; Frère, P.; Garrigues, B.; Gorgues, A.; Jubault, M.; Carlier, R.; Texier, F. *Tetrahedron Lett.* **1992**, *33*, 6457.
(10) Hansen, T. K.; Lakshmikantham, M. V.; Cava, M. P.; Niziurski-Man, R. E.; Jensen, F.; Becher, J. *J. Am. Chem. Soc.* **1992**, *114*, 5035.
(11) Yamashita, Y.; Kobayashi, Y.; Miyashi, T. *Angew. Chem., Int. Ed. Engl.* **1989**, *28*, 1052.
(12) Bryce, M. R.; Moore, A. J.; Hasan, M.; Ashwell, G. J.; Fraser, A. T.; Clegg, W.; Hursthouse, M. B.; Karaulov, A. I. *Angew. Chem., Int. Ed. Engl.* **1990**, *29*, 1450. Moore, A. J.; Bryce, M. R. *J. Chem. Soc., Perkin Trans. 1* **1991**, 157.
(13) Triki, S.; Ovahab, L.; Lorcy, D.; Robert, A. *Acta Crystallogr. C* **1993**, *49*, 1189.
(14) Suchanski, M. R.; Van Duyne, R. P. *J. Am. Chem. Soc.* **1976**, *98*, 250.
(15) Robert, A.; Lorcy, D. In *Molecular Engineering for Advanced Materials*; Becher, J., Schaumberg, K., Eds.; Kluber: Dordrecht, 1995; p 251.
(16) Martín, N.; Pérez, I.; Sánchez, L.; Seoane, C. *J. Org. Chem.* **1997**, *62*, 870.
(17) Yamashita, Y.; Tanaka, S.; Imaeda, K.; Inokuchi, H. *Chem. Lett.* **1991**, 1213. Yamashita, Y.; Tanaka, S.; Imaeda, K.; Inokuchi, H.; Sano, M. *J. Org. Chem.* **1992**, *57*, 5517. See also: Yamashita, Y.; Tomura, M.; Imaeda, K. *Chem. Commun.* **1996**, 2021.
(18) Martín, N.; Sánchez, L.; Seoane, C.; Fernández, C. *Synth. Met.* **1996**, *78*, 137.
(19) Orduna, J.; Garín, J.; Frère, P.; Nguyen, T.; Gorgues, A.; Sánchez, L.; Martín, N.; Seoane, C. *Rapid. Commun. Mass. Spectrom.* **1995**, *9*, 856.

Scheme 1

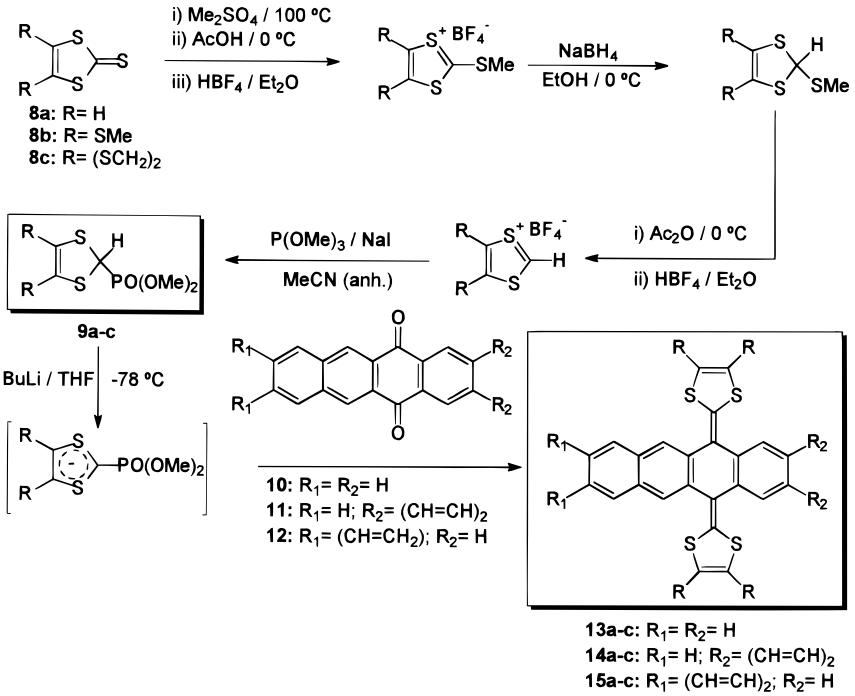

substituents on the 1,3-dithiole rings. Cyclic voltammetry and UV−vis spectroscopic measurements are combined with quantum-chemical calculations to characterize the compounds prepared.

Results and Discussion

Synthesis. The preparation of the novel π-extended donors (**13**−**15**) was carried out according to Scheme 1. We have proved the usefulness of the Wittig−Horner reaction of the carbanion, generated from phosphonate esters **9a**−**c** in the presence of *n*-butyllithium at −78 °C, with the respective acenequinones (**10**−**12**), despite the poor solubility of these highly conjugated quinonic systems in the usual organic solvents.

Phosphonate esters (**9a**−**c**) were prepared in several steps by following well-established procedures[20] from substituted 1,3-dithiole-2-thiones (**8a**−**c**), which were in turn obtained by using literature procedures.[21] Largely π-extended quinones were commercially available or prepared by previously reported procedures.[22] The electron-donor compounds (**13**−**15**) were obtained as air-stable orange solids in moderate to good yields (see the Experimental Section). These compounds showed low solubility in common organic solvents and, particularly, those derived from the BEDT-TTF for which the ^{13}C NMR spectra could not be recorded due to their rather poor solubility.

The analytical and spectroscopic data clearly support the proposed structures. The UV−vis spectra recorded for the extended donors **13**−**15** show that the lowest-energy absorption band appearing above 400 nm is, as expected, bathochromicly shifted in comparison to the parent TTF, but it is blue-shifted with respect to **5a** (see Table 1). These shifts indicate that part of the π-conjugation gained by **5a** with respect to TTF is lost in compounds **13**−**15**. The λ_{max} value is slightly shifted to the red when the dithiole rings bear electron-releasing substituents. It also depends on the number of benzene rings fused to the quinonoid structure. λ_{max} for donors **15a**−**c**, bearing anthracene and benzene moieties laterally fused to the *p*-quinodimethane system, is red-shifted compared to compounds **13** and **14**, which hold one naphthalene and one benzene unit, and two naphthalene units fused in their structures, respectively. This finding suggests the existence of a photoinduced intramolecular electron transfer in compounds **15** from the donor *p*-quinodimethane-extended TTF to the anthracene fragments, acting as the acceptor part of the molecule (Figure 1). This feature has also been suggested in other simpler, highly conjugated π-electron donors bearing the electron-withdrawing thiadiazole ring.[23] UV−vis data are discussed below on the basis of theoretical calculations carried out on the unsubstituted derivatives **6a**, **13a**, **14a**, and **15a**.

Electrochemistry. The redox potentials of compounds **13**−**15** were determined by cyclic voltammetry (CV) measurements, carried out in methylene dichloride at room temperature with tetrabutylammonium perchlorate as the supporting electrolyte. All of them show the presence of two oxidation waves (Figure 2a), the first one corresponding to a quasireversible oxidation wave involving two electrons to the formation of the dication. This electrochemical behavior is in agreement with that previously observed for the anthracenediylidene derivative **6a**, the coulometric analysis of which confirmed the two-electron nature of the process.[12] The coalescence of the first oxidation process of TTF,[1] which appears more closely located for the quinonoid extended TTF **5a**,[11] under a single two-electron wave clearly indicates that

(20) Akiba, K.; Ishikawa, K.; Inamoto, N. *Bull. Chem. Soc. Jpn.* **1978**, *51*, 2674. Moore, A. J.; Bryce, M. R. *Synthesis* **1991**, 26.

(21) Steimecke, G.; Sieler, H.; Kirmse, R.; Hoyer, E. *Phosphorus Sulfur* **1979**, *7*, 49. Sukumar, K.; Bury, A.; Harris, N. J.; Underhill, A. E. *Synthesis* **1987**, 837.

(22) Ried, W.; Anthöfer, F. *Angew. Chem.* **1953**, *65*, 601. Serpaud, B.; Lepage, Y. *Bull. Chim. Fr.* **1977**, *5*−*6*, 539.

(23) Yamashita, Y.; Tanaka, S.; Imaeda, K.; Inokuchi, H.; Sano, M. *Chem. Lett.* **1992**, 419.

Table 1. Cyclic Voltammetry at Room Temperature and UV−Vis Data for Compounds 13−15

Compound	Formula	$E^1_{½oxid}$ [a]	$E^2_{a.p.}$ [a]	λ_{max} (nm)[b]
TTF		0.37	0.67	317[c]
5a	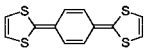	-0.11[d]	-0.04[d]	495[d]
6a	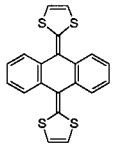	0.44	—	415
13a: R=H	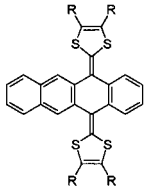	0.39	1.47	417
13b: R=SMe		0.55	1.47	422
13c: R,R=$(SCH_2)_2$		0.52	1.45	434
14a: R=H	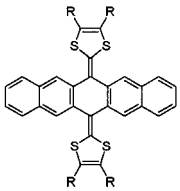	0.50	1.48	404
14b: R=SMe		0.63	1.41	406
14c: R,R=$(SCH_2)_2$		0.65	1.41	420
15a: R=H	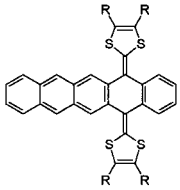	0.49	1.31	458
15b: R=SMe		0.59	—	460
15c: R,R= $(SCH_2)_2$		0.59	—	462
Anthracene	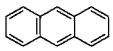	—	1,40	
Naphthacene	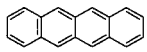	—	1.03	

[a] Experimental conditions: CH_2Cl_2, V *vs* SCE, GCE as working electrode, NBu_4^+ ClO_4^- as supporting electrolite, scan rate: 200 mV/s. [b] in CH_2Cl_2. [c] Coffen, D. L. Chambers, J. Q.; Williams, D. R.; Garrett, P.E.; Canfiled, N. D. *J. Am. Chem. Soc.* **1971**, *93*, 2258. [d] ref. 11

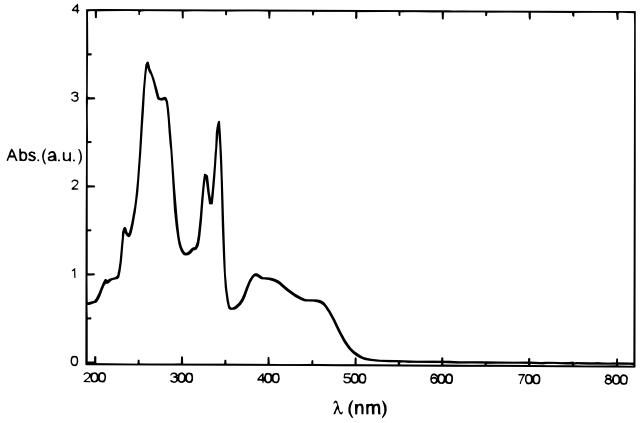

Figure 1. UV−vis spectrum of compound **15b** in CH_2Cl_2

benzoannulation leads to a decreasing of the stability of the radical-cation, thus more readily forming the respective dications. The first oxidation potential values found for **13**−**15** are slightly higher than that found for the parent TTF under the same experimental conditions. Although the introduction by Yamashita et al.[11] of the *p*-quinodimethane spacer between the two dithiole rings increases the donor ability of compound **5a**, in comparison with TTF, the presence of two laterally fused benzene rings resulted in the formation of poorer donors.[12] Further extension of the π-conjugation with naphthalene or anthracene units decreases only very slightly the donor character and the presence of two naphthalene fragments laterally fused to the *p*-quinodimethane moiety leads to the most positive oxidation potential values (see Table 1). Similarly to TTF derivatives, the presence of methylthio or ethylenedithio groups as substituents on the dithiole rings results in a shift of the oxidation potential toward more positive values. It is worth mentioning that although these compounds do not form stable cation radicals, the second electron is donated more easily than in the parent TTF, because of the lower on-site Coulomb repulsion.

The second irreversible oxidation wave observed at about 1.3−1.4 V for compounds **13**−**15** has been assigned to the oxidation of the hydrocarbon framework to form the trication-radical. The values found for the second oxidation potential of **13a**−**c** are higher than that observed for unsubstituted naphthacene under the same

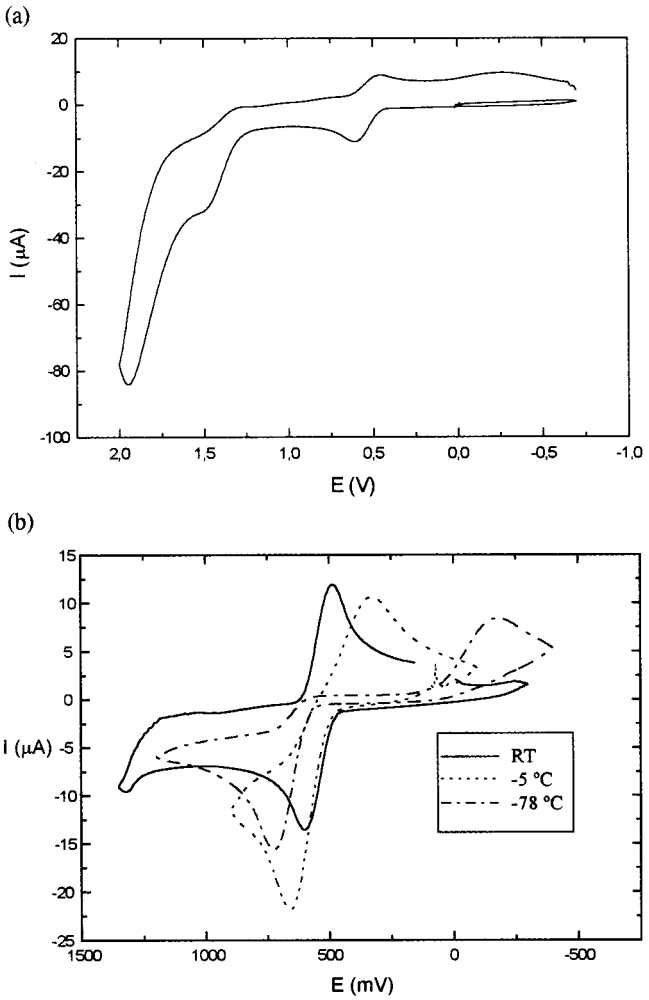

Figure 2. (a) Room-temperature cyclic voltammogram of **13b**. (b) Temperature-dependent cyclic voltammograms of compound **13b**.

experimental conditions. The values recorded for **14** and **15** are similar or slightly lower than those measured for **13** and would be higher than the first oxidation potential expected for pentacene. The extremely low solubility of pentacene precludes a reliable estimate of its redox potentials, but it is perfectly stablished that both the oxidation and reduction potentials decrease along the acene series.[24] These findings could be accounted for by the fact that two positive charges are already present in the system, thus making the oxidation of the polyacenic framework more difficult since it implies the introduction of a third positive charge in the neighborhood. The lower solubility of the pentacene derivatives **14** and **15** prevented the accurate determination of their second oxidation potential values.

The electrochemical redox behavior of compound **13b** was studied at different temperatures, and the voltammograms recorded at room temperature, −5 °C, and −78 °C are shown in Figure 2b. The oxidation potential values are anodically shifted with decreasing the temperature [$E_{ox(rt)} = 0.607$ V; $E_{ox(-5°C)} = 0.698$ V; $E_{ox(-78°C)} = 0.725$ V], which indicates a higher difficulty in the formation of the dication species. A much more striking effect is observed in the reduction wave associated to the process donor$^{2+} \rightarrow$ donor^0, which undergoes a drastic shift to lower potentials when lowering the temperature [$E_{red(rt)} = 0.487$ V; $E_{red(-5°C)} = 0.263$ V; $E_{red(-78°C)} = -0.175$ V]. This shift was previously reported by Bryce et al.[12] for compounds **6** and was interpreted as an indication of the high stability of the respective dications. This reasoning was later supported by X-ray analysis of compound **6b**, which was found to show a highly distorted geometry in the neutral form and a planar anthracene moiety with the 1,3-dithiole rings in almost an orthogonal position (86.0°) in the dication form.[12]

Table 2. Spectroscopic and Analytical Data of Novel Complexes Prepared

complex	ν_{CN}[a] (cm^{-1})	λ_{max}[b] (nm)	stoichiometry[c] (D:A:CH_2Cl_2)
13b·$TCNQF_4$	2193, 2174	685, 752, 855	1:2:1
13c·$TCNQF_4$	2196, 2174	686, 753, 855	1:2:0.5
14b·$TCNQF_4$	2192, 2174	683, 752, 855	1:2:0.5
14c·TCNQF4	2197, 2174	684, 753, 855	1:2:2

[a] FT-IR (KBr disk). [b] Solvent: MeCN. [c] Deduced from elemental analysis.

The location of the respective reduction waves in compounds **13**−**15** at similar potential values indicates that substitution on the 1,3-dithiole rings or a further enlargement of benzoannulation do not significantly alter the required energy to go from the stable dication to the highly distorted neutral form. The formation of the dication is discussed below on the basis of theoretical calculations.

As shown in Figure 2a for **13b**, the π-extended donors **13**−**15** exhibit an intense reduction wave at negative voltages. The wave only appears when oxidation is undertaken until the dication is generated and is not observed when oxidation is stopped after the dication is obtained. These findings indicate that the reduction wave is not associated to the dication and should be attributed to an electrochemical process related to the trication. It should be also mentioned that when the trication is generated, the formation of the dication becomes more irreversible since the corresponding reduction wave is cathodically shifted.

Charge-Transfer Complexes. The novel donor compounds **13** and **14** did not form CT-complexes with TCNQ as the acceptor molecule. However, they were found to form crystalline CT-complexes with the stronger acceptor 2,3,5,6-tetrafluorotetracyano-*p*-quinodimethane ($TCNQF_4$) in refluxing methylene dichloride. It was not possible to obtain appropriate crystals for X-ray analysis and single crystals for conductivity measurements. The spectroscopic and analytical data registered for the complexes formed are summarized in Table 2. The IR spectra show two cyanide absorptions, thus indicating the presence of ionic $TCNQF_4$ molecules. The existence of charge transfer was also confirmed by the presence of several electronic transitions in the visible region of the UV−vis spectra recorded in acetonitrile solution. The stoichiometry of these complexes shows a 1:2 (D:A) ratio, with a variable amount of solvent molecules.[25] These results were further confirmed by repeating the elemental analyses at several days intervals of time drying under pump vacuum. Attemps to form CT-complexes with donors **13b,c** and **14b,c** in acetonitrile were met with futility due to their poor solubility in this solvent.

(24) Pysh, E. S.; Yang, N. C. *J. Am. Chem. Soc.* **1963**, *85*, 2124. Kubota, T.; Kano, K.; Uno, B.; Konse, T. *Bull. Chem. Soc. Jpn.* **1987**, *60*, 3865. Boschi, R.; Clar, E.; Schmidt, W. *J. Chem. Phys.* **1974**, *60*, 4406.

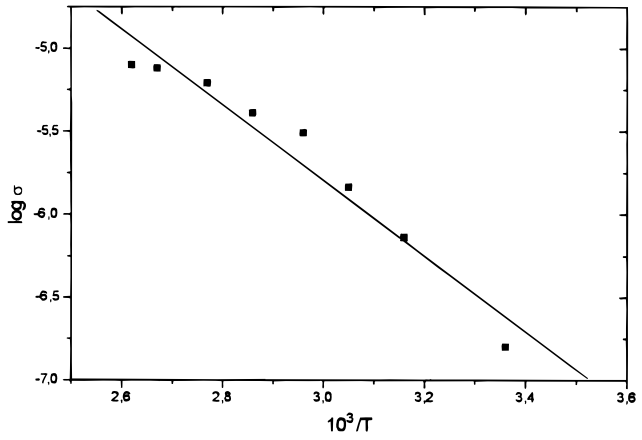

Figure 3. Temperature dependence of electrical conductivity of complex **13c**·$TCNQF_4$.

Conductivity measurements were carried out for complexes **13c**·$TCNQF_4$ and **14c**·$TCNQF_4$ and were made on compressed pellets using the two-probe technique. A conductivity of 10^{-6} S·cm^{-1} was recorded for **14c**·$TCNQF_4$ at room temperature. This is a typical value for organic semiconducting CT-complexes. The temperature dependence of the conductivity for **13c**·$TCNQF_4$ is shown in Figure 3. This complex has a conductivity of 10^{-5} S·cm^{-1} at 380 K and exhibits a semiconducting behavior with an activation energy (E_a) of 0.49 eV.

Theoretical Calculations. To gain a deeper understanding of the experimental observations discussed above, the molecular structure and electronic properties of the unsubstituted compounds **5a**, **6a**, **13a**, **14a**, and **15a** on both neutral and oxidized states were theoretically investigated using different quantum-chemical approaches. Compounds **5a** and **6a** are used as reference systems with respect to which the properties calculated for the more extended TTF derivatives should be compared.

1. Molecular Structure. Due to the large size of the systems studied calibration calculations using different theoretical approaches were first performed for compound **6a**, for which experimental structural data are available. This section is thus structured as follows. The molecular structures calculated for **6a** at the semiempirical PM3 level and at the more accurate ab initio Hartree−Fock (HF/6-31G*) and density functional theory (DFT, B3-P86/6-31G*) levels are first discussed and compared in order to check the reliability of the PM3 method in dealing with the geometries of the more extended systems. The results obtained for compounds **13**−**15** are next analyzed.

The geometry of **6a** was optimized assuming a D_{2h} planar symmetry and allowing the molecule to lose planarity within different symmetry restrictions. Table 3 summarizes the geometrical parameters obtained at the PM3, HF/6-31G*, and B3-P86/6-31G* levels for the minimum-energy C_{2v} conformation depicted in Figure 4. Table 3 further includes the X-ray data reported by Bryce et al.[12] for **6b** for the sake of comparison. The atom numbering used in this section corresponds to that depicted in Figure 4.

As can be seen from Figure 4 and Table 3, the outer benzene rings of **6a** preserve their aromaticity, the carbon−carbon bonds having a length of 1.40 ± 0.01 Å and the internal bond angles being 120 ± 1°. The quinonoid character of the central ring is thus reduced with respect to **5a**, since the C2−C3 and C5−C6 bonds are lengthened from 1.345 Å for **5a** to 1.409 Å for **6a** (PM3 level). As a consequence, the C1−C2 (1.472 Å) and C1−C7 (1.354 Å) bonds slightly increase their respective single- and double-bond character compared to **5a** (1.454 and 1.361 Å, respectively). The dithiole rings have bond lengths and bond angles very similar to those obtained for these rings in **5a**. These trends are independent of the theoretical level used and agree with those observed from X-ray data.[12]

The average deviations between the experimental data reported for **6b** and the theoretical parameters calculated for **6a** are given in Table 3 for the bond lengths $\bar{\delta}(R)$, and the bond angles, $\bar{\delta}(\beta)$. The deviations are found to be small, the minimum values corresponding to the B3−P86/6-31G* calculations, which include electron correlation effects, and the maximum values to HF/6-31G* calculations, which provide a too localized structure. These results show the agreement between theory and experiment and demonstrate that the PM3 method provides a good description, even better than ab initio HF/6-31G* calculations, of the molecular structure of extended TTFs. It should be noted that the geometry of **6b** was also optimized at the PM3 level to investigate the effect of the substituents. The geometry calculated is almost identical with that presented in Table 3 for unsubstituted **6a**, showing that the substituents have almost no influence on the molecular geometry. The deviations from X-ray data are reduced to = 0.017 Å and = 1.4°.

As shown in Figure 4, the minimum-energy conformation of **6a** corresponds to a butterfly-shaped nonplanar structure. The planar conformation of the molecule is strongly hindered by the very short contacts between the sulfur atoms and the hydrogen atoms in peri positions, which, at the PM3 level, are calculated to be at 1.78 Å, i.e., half of the van der Waals distance (3.60 Å).[26] To avoid these interactions, the central ring folds into a boat conformation and the molecule adopts a butterfly structure where the benzene rings point upward and the dithiole rings point downward. The resulting conformation exactly corresponds to that observed for **6b** in the crystal.[12]

Distortions from planarity can be described in terms of angles α and γ. Angle α corresponds to the angle formed by the outer benzene rings, i.e., by the "wings of the butterfly", while γ defines the tilting of the dithiole units and is obtained as the supplement of the C7−C2−C6−C5 dihedral angle. Table 4 collects the values calculated for α and γ. For **6a**, they have values of 139.0° and 34.8° at the PM3 level (identical values are obtained for **6b** thus confirming the small effect that substitution has on the molecular structure), 136.3° and 39.4° at the ab initio HF/6-31G* level, and 142.1° and 34.0° at the B3-P86/6-31G* level. All these values are close to those obtained from X-ray data (143.8° and 33.3°, respectively), and it is not possible to discriminate which method provides the better estimates since calculations are performed on isolated systems and the experimental

(25) We have found that the solvent has a striking influence on the stoichiometry of the complex formed. The previously reported 1:3 (D:A) complex **13a**·$TCNQF_4$ in MeCN[18] shows a 1:2 (D:A) ratio containing half molecule of the CH_2Cl_2 solvent. Anal. Calcd for $C_{97}H_{34}N_{16}F_{16}S_8Cl_2$: C, 56.70; H, 1.67; N, 10.91. Found: C, 57.05; H, 1.30; N, 11.02.

(26) Rowland, R. S.; Taylor, R. *J. Phys. Chem.* **1996**, *100*, 7384.

Table 3. Bond Lengths (Å) and Bond Angles (Deg) Calculated for 6a and Its Dication at Different Theoretical Levels

	6a				**6a**$^{2+}$			
parameters[a]	PM3	6-31G*	B3-P86	X-ray[b]	PM3	6-31G*	B3−P86	X-ray[c]
C1−C2	1.472	1.491	1.473	1.477	1.410	1.400	1.411	1.402
C2−C3	1.409	1.403	1.412	1.413	1.425	1.428	1.442	1.430
C1−C7	1.354	1.334	1.363	1.343	1.470	1.496	1.478	1.487
C7−S9	1.780	1.785	1.778	1.758	1.691	1.674	1.694	1.665
S9−C13	1.739	1.755	1.747	1.793	1.702	1.723	1.718	1.711
C13−C14	1.340	1.315	1.336	1.345	1.366	1.355	1.356	1.339
C2−C17	1.394	1.386	1.398	1.421	1.433	1.437	1.424	1.427
C17−C18	1.391	1.387	1.392	1.418	1.361	1.347	1.367	1.363
C18−C19	1.390	1.381	1.391	1.406	1.424	1.427	1.417	1.382
C6−C1−C2	111.8	112.1	113.8	114.8	120.7	122.7	122.4	121.9
C1−C2−C3	117.9	116.7	117.7	117.6	119.7	118.7	118.8	119.0
C1−C7−C9	123.8	123.9	123.8	124.5	121.1	122.3	122.6	122.7
S9−C7−S10	112.4	112.1	112.3	110.9	117.8	115.4	114.8	114.7
C7−S9−C13	96.1	95.7	95.9	98.5	94.4	96.6	96.7	97.3
S9−C13−C14	117.7	117.9	117.6	115.6	116.7	115.7	115.9	115.3
C3−C2−C17	119.6	119.5	119.0	120.7	118.4	118.3	118.4	118.7
C2−C17−C18	120.2	120.6	121.2	118.4	121.6	121.3	121.2	120.0
C17−C18−C19	120.2	120.0	119.8	120.9	120.1	120.4	120.3	121.3
$\bar{\delta}(R)$[d]	0.019	0.024	0.018		0.016	0.014	0.014	
$\bar{\delta}(\beta)$[d]	1.51	1.64	1.49		1.60	0.64	0.54	

[a] The number of atoms is given in Figure 4. [b] X-ray data for **6b** from ref 12. [c] X-ray data for **6b**$^{2+}$ in the 1:4 TCNQ complex from ref 12. [d] Average deviations calculated for bond lengths, $\vartheta(R)$, and bond angles $\delta(\beta)$, with respect to X-ray values.

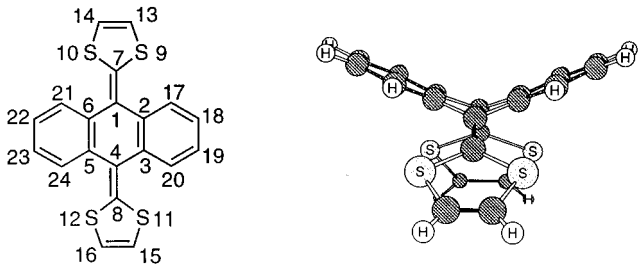

Figure 4. Atom numbering used in the text (left). Butterfly shaped, minimum-energy conformation (C_{2v} symmetry) calculated for **6a**.

values are taken from the crystal where the packing forces tend to planarize the molecules to achieve the most compact packing.

Figure 5 displays the PM3-optimized geometries of **13a**, **14a**, and **15a**. The geometries of **13a** and **15a** were calculated by assuming a C_s symmetry, while a higher C_{2v} symmetry was imposed for **14a**. The PM3 geometries obtained for naphthalene and anthracene molecules (D_{2h} symmetry) are included in Figure 5 for comparison purposes. The 1,3-dithiol-2-ylidene moieties present identical geometries in all cases. As for **6a**, the laterally fused benzene, naphthalene, and/or anthracene units preserve their structural identity. The bond lengths and bond angles calculated for the naphthalene moieties in **13a** and **14a** are identical with those obtained for the naphthalene molecule, and only the C−C bond fusing the naphthalene unit to the central ring presents a deviation of ca. 0.02 Å. A similar correlation is observed between **15a** and the anthracene molecule.

Compounds **13a**−**15a** adopt a butterfly-like structure identical with that of **6a**. The values collected in Table 4 for angles α and γ indicate that the distortions from planarity slightly increase by ca. 1°, when the laterally fused polyacenic units are extended. These units always preserve their planarity. From a structural standpoint, the π-extended TTF studied here can be therefore visualized as being formed by polyaromatic units (benzene, naphthalene, and anthracene) linked together by 1,3-dithiol-2-ylidene units. The consequences of these structural findings on the electronic properties are discussed below.

2. Electronic Structure. The electronic structure was calculated using the PM3-optimized geometries and the nonempirical VEH pseudopotential technique. Compared to standard ab initio calculations, the VEH method yields one-electron molecular orbital energies of double-ζ quality and has the advantage of providing good estimates for the lowest-energy optical transitions.[27] This feature is due to the fact that the VEH parametrization is not contaminated by any information coming from the unoccupied Hartree−Fock molecular orbitals (MOs), which are always calculated as being too high in energy. As a consequence, the energies of the virtual MOs afforded by the VEH method are expected to be of the same quality as for the occupied MOs.

Figure 6 correlates the energy and atomic (AO) composition calculated at the VEH level for the HOMOs and LUMOs of **5a**, **6a**, **13a**, **14a**, and **15a**. The HOMO (−7.16 eV) and LUMO (−4.16 eV) of **6a** preserve the AO composition of the HOMO (−6.71 eV) and LUMO (−4.70 eV) of **5a**. The shifts of the HOMO of **6a** to lower energies and of the LUMO to higher energies are a consequence of the loss of planarity of the central quinone ring, which modifies the bonding/antibonding interactions. Since oxidation implies the extraction of an electron from the HOMO, more positive oxidation potentials are therefore to be expected for compounds with lower energy HOMOs. The stabilization of the HOMO thus justifies, in a first approach, the more positive oxidation potential recorded for **6a** compared to **5a** (see Table 1). The HOMO of **6a** in fact appears at an energy (−7.16 eV) almost identical with that of the HOMO of the parent TTF (−7.14 eV, VEH level), accounting for the very similar oxidation potentials measured for both compounds (0.37 and 0.44 V, respectively). In passing to the more extended systems **13a**, **14a**, and **15a**, the energy of the HOMO remains almost constant since it is mostly localized on the 1,3-dithiol-2-ylidene moieties (see Figure 6). This result supports the fact that the oxidation potential remains

Table 4. Optimized Angles (Deg) Defining the Molecular Distortions from Planarity of π-Extended TTF Derivatives

	α^a			γ^a		
molecule	PM3	6-31G*	B3−P86	PM3	6-31G*	B3−P86
6a	139.0	136.3	142.1	34.8	39.4	34.0
6b	139.0 (143.8)[b]			34.8 (33.3)[b]		
13a	138.5			35.3		
14a	137.9			35.8		
15a	138.3			35.4		

[a] Angles α and γ are defined in the text. [b] X−ray data from ref 12.

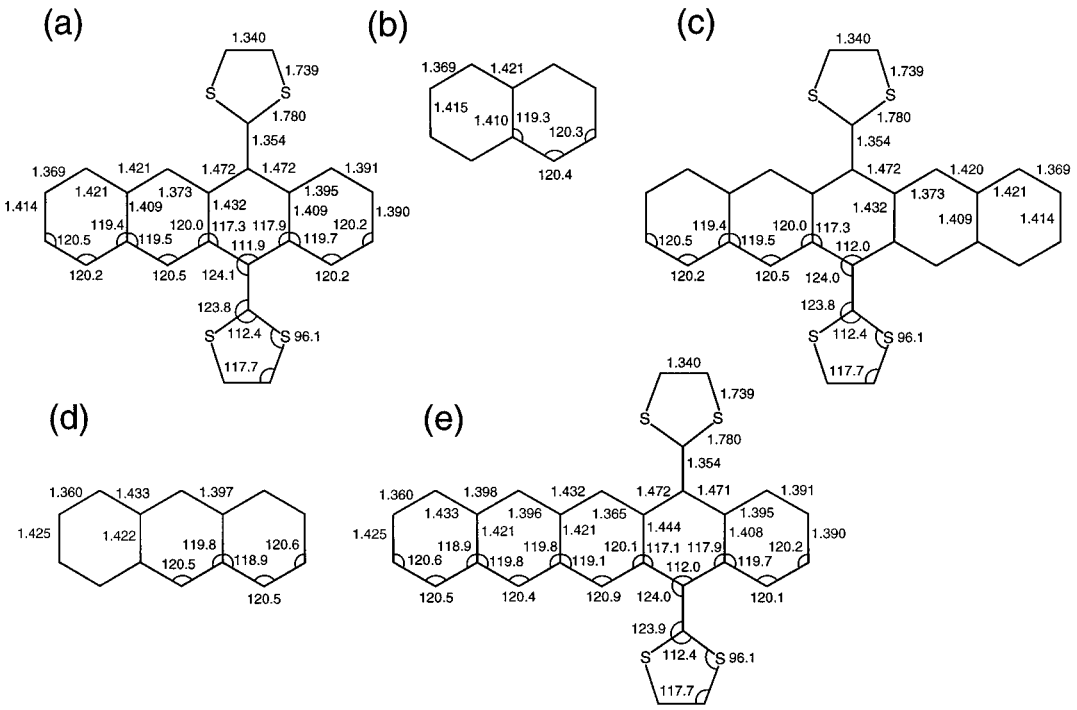

Figure 5. PM3-optimized bond lengths (Å) and bond angles (deg) for (a) **13a** (C_s symmetry), (b) naphthalene (D_{2h} symmetry), (c) **14a** (C_{2v} symmetry), (d) anthracene (D_{2h} symmetry), and (e) **15a** (C_s symmetry).

almost unchanged in going from **6a** to the more extended systems (Table 1).

Regarding the optical properties, the stabilization of the HOMO together with the destabilization of the LUMO determine that the HOMO−LUMO energy gap increases in passing from **5a** to **6a**. This result explains the blue shift observed for the first absorption band of **6a** in the UV−vis spectra (see Table 1). The HOMO−LUMO energy gap is predicted to have a value of 3.00 eV (413 nm) for **6a**, in good agreement with the wavelength recorded for the lowest-energy absorption band (415 nm).

For **13a**, the LUMO (−4.08 eV) retains the same topology as for **6a** and another orbital, the LUMO+1, appears very close in energy (−4.07 eV). These findings justify the observation of the first absorption band (417 nm) at similar wavelengths as for **6a** (415 nm) and the appearance of a second band close in energy (385 nm). It is to be stressed that the LUMO+1 is located on the naphthalene moiety, and its topology corresponds to that of the LUMO of the naphthalene molecule. This means that the HOMO → LUMO+1 electronic transition actually implies an electron transfer from the 1,3-dithiol-2-ylidene units where the HOMO is located to the naphthalene fragment acting as the acceptor. A similar situation is calculated for **14a**, for which the LUMO is now located on the naphthalene units and the LUMO+1 correlates with the LUMO of **6a**. Theoretical calculations thus suggest that one of the two first absorption bands observed close in energy for compounds **13** and **14** corresponds to an intramolecular charge-transfer band.

The nature of the absorption bands can be more easily established for compounds **15**. As can be seen from Figure 6, the LUMO of **15a** now lies clearly separated from the LUMO+1. It is located on the laterally fused anthracene unit and appears at an energy (−4.63 eV) almost identical with that calculated for the LUMO of the anthracene molecule (−4.58 eV). The HOMO → LUMO electronic transition thus appears at lower energies (2.59 eV, 479 nm) due to the lower energy of the LUMO of anthracene. This explains the red shift observed for the first absorption band of **15a** (458 nm), which has to be assigned to an intramolecular charge-transfer band. The second absorption band (384 nm) corresponds to the HOMO → LUMO+1 transition (3.17 eV, 391 nm) and correlates with the first absorption band of **6a**.

Lateral benzoannulation therefore introduces new low energy orbitals around or below the LUMO of **6a**. These orbitals belong to the lateral polyacenic units, which preserve not only their structural but also their electronic identity and decrease in energy as the length of these units increases. As a consequence, intramolecular charge-transfer bands appear for largely π-extended TTFs due to the electron transfer between the 1,3-dithiol-2-ylidene units and the laterally fused polyacenic units. This

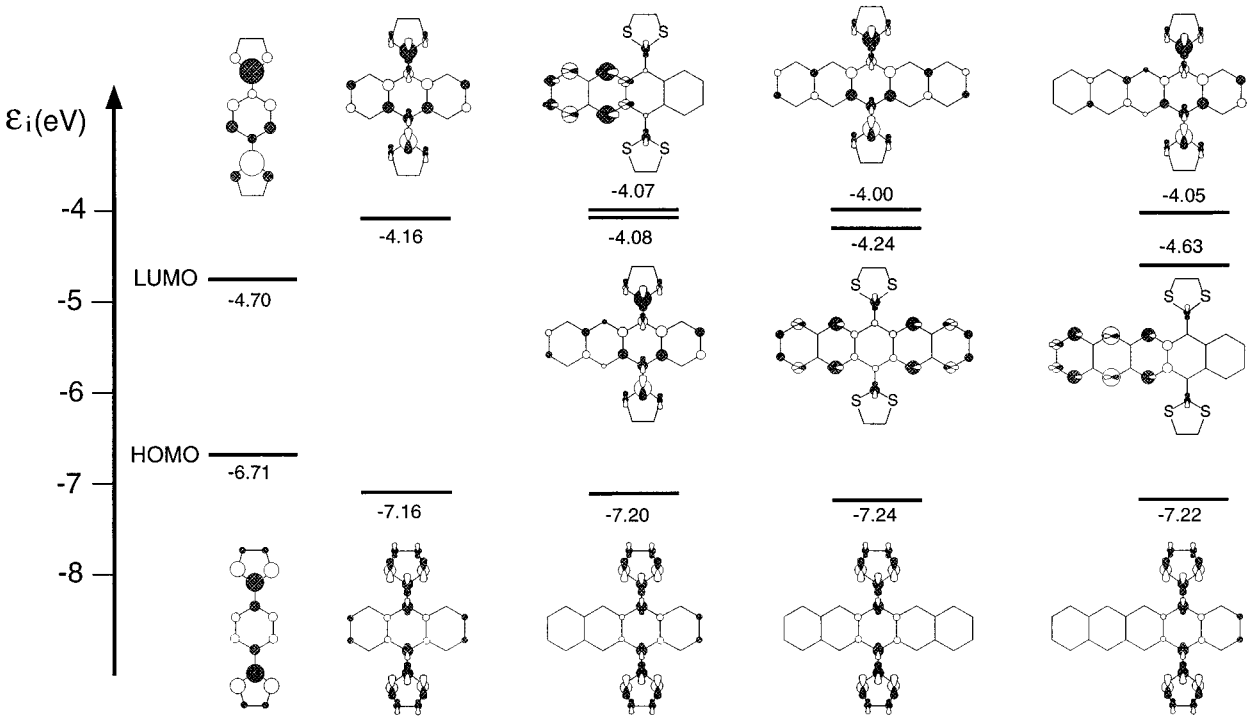

Figure 6. Molecular orbital diagram correlating the energies and atomic orbital (AO) compositions of the HOMO and LUMO calculated for **5a**, **6a**, **13a**, **14a**, and **15a** at the VEH level. Contributions from AOs other than π-type orbitals are due to the nonplanarity of the molecule.

charge-transfer band is not observed for compounds **6** because the lateral benzene moieties are not as good acceptors as the naphthalene or anthracene units present in the more extended systems. A similar effect was previously discussed for the optical properties of laterally benzoannulated TCNQ derivatives for which the polyacenic fragments played the role of donor units in the electron-transfer bands.[28]

3. Oxidized Compounds. To get a deeper insight into the oxidation process and how it affects the molecular and electronic structures, the geometries of the cation and dication of **6a** were optimized using the PM3 method and HF/6-31G* and B3-P86/6-31G* calculations. Table 3 collects the bond lengths and bond angles calculated for the dication together with the X-ray data obtained for $6b^{2+}$ from the 1:4 complex formed with TCNQ.[12]

The oxidation process mainly affects the central quinone ring and the dithiole units since the HOMO, i.e., the orbital from which electrons are removed, is mostly located on these moieties. At the PM3 level, the C2−C3 and C5−C6 bonds lengthen from 1.409 Å in neutral **6a** to 1.425 Å for $\mathbf{6a}^{2+}$, while the C1−C2,C6 and C4−C3,C5 bonds shorten from 1.472 to 1.410 Å. The exocyclic C1−C7 and C4−C8 bonds undergo the largest change, increasing by 0.116 Å, and the C7−S and C8−S bonds decrease by 0.078 Å. All these changes are reproduced at the more accurate HF/6-31G* and B3−P86/6-31G* levels and are in accord with the experimental X-ray data.[12] The mean deviations between the experimental and the calculated parameters, $\bar{\delta}(R)$ and $\bar{\delta}(\beta)$, are similar for all three theoretical approaches used (see Table 3), showing the reliability of the PM3 predictions.

The aromatization of the quinone and dithiole rings during the oxidation process has important consequences on the conformation adopted by the molecule. After

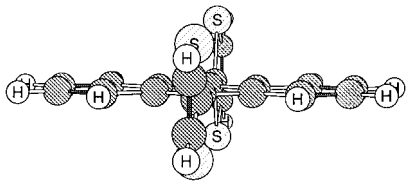

Figure 7. PM3-minimun-energy conformation calculated for $\mathbf{6a}^{2+}$.

removal of the first electron to form the cation, the molecule slightly reduces the distortions from planarity by increasing α from 142.1° to 146.2° and decreasing γ from 34.0° to 31.3°, but it preserves the butterfly-shaped conformation observed for the neutral system. The extraction of the second electron to form the dication affects more drastically the molecular conformation. As shown in Figure 7, the central anthracene backbone is now completely planar. This planarization is made possible by the lengthening of the exocyclic C1−C7 and C4−C8 bonds, which exhibit a marked single-bond character for the dication (1.470 Å at the PM3 level) and allow for the rotation of the dithiole rings out of the molecular plane, thus avoiding the steric interactions of the sulfur atoms with the hydrogen atoms in peri positions. Both the PM3 approach and the HF/6-31G* and B3-P86/6-31G* calculations predict that the dithiole rings adopt an orthogonal disposition with respect to the anthracene plane in accord with the twisting angles of 86.0° and 92° reported for $\mathbf{6b}^{2+}$ and for a dithiomethyl derivative[29]from X-ray analysis.[12] The geometries of the

(27) Brédas, J. L.; Thémans, B.; André, J. M. *J. Chem. Phys.* **1983**, *70*, 6137. Viruela, R.; Viruela, P. M.; Ortí, E. *J. Chem. Phys.* **1992**, *97*, 8470.

(28) Ortí, E.; Viruela, R.; Viruela, P. M. *J. Mater. Chem.* **1995**, *5*, 1697. Martín, N.; Segura, J. L.; Seoane, C.; de la Cruz, P.; Langa, F.; Ortí, E.; Viruela, P. M.; Viruela, R. *J. Org. Chem.* **1995**, *60*, 4077.

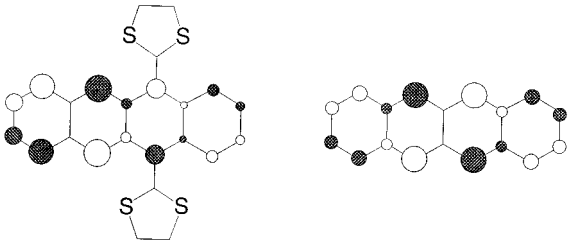

Figure 8. AO composition of the HOMO of $\mathbf{13a}^{2+}$ (left) and naphthacene (right).

cations and dications of compounds **13a**, **14a**, and **15a** were optimized at the PM3 level and show the same trends discussed for **6a**.

It is important to note that the planar polyacenic units linking the two dithiole rings in the dications of **6a**, **13a**, **14a**, and **15a** exhibit almost exactly the same geometry as those calculated for anthracene ($\mathbf{6a}^{2+}$), naphthacene ($\mathbf{13a}^{2+}$), and pentacene ($\mathbf{14a}^{2+}$ and $\mathbf{15a}^{2+}$) molecules. This can be verified by comparing the geometric parameters given in Table 3 for $\mathbf{6a}^{2+}$ and those displayed in Figure 5d for neutral anthracene. This finding suggests that the electrons in the dication are mainly removed from the dithiole rings and that the polyacenic unit remains almost neutral. The analysis of the net atomic charge distributions calculated at the PM3 level confirms this suggestion since each dithiole ring in the dication accumulates an extra positive charge of 0.94 e. The dications of the extended TTFs studied here have, therefore, to be visualized as a central polyacenic unit substituted by two singly charged dithiole rings orthogonal to the molecular plane. Each of these dithiole rings has six π-electrons and shows an aromatic character.

The structural characteristics calculated for **6a**, **13a**, **14a**, and **15a** in neutral and oxidized states explain the electrochemical behavior exhibited by these extended TTFs. The gain in aromaticity in going from the neutral molecule to the cation is small because the cation remains highly distorted from planarity. By contrast, the dication is formed by three aromatic units: the central polyacenic moiety and the two singly charged dithiole rings. This implies that the cation is destabilized with respect to the dication, thus explaining the anodic shift of the first oxidation potential and its collapse with the second oxidation potential under the same CV wave observed experimentally. The irreversibility of this wave and the shift of the reduction peak to more negative values as the temperature is decreased (see Figure 2) is, as suggested by Bryce et al. for compounds **6**,[12,30] due to the marked conformational change that must take place on reduction (planar anthracene → buckled anthraquinodimethane), which involves the loss of aromaticity of all three constituting units.

We finally discuss the formation of more highly charged species for benzoannulated TTFs. For the dication, the 1,3-dithiolium rings are perpendicular to the molecular plane and their interaction with the polyacenic unit is small. The electronic properties of the dications are thus dominated by those of the polyacenic unit. This is shown in Figure 8, which displays the atomic orbital composition of the HOMOs of $\mathbf{13a}^{2+}$ and naphthacene. The HOMO of $\mathbf{13a}^{2+}$ has no contribution from the dithiolium rings and its topology exactly corresponds to that of the HOMO of anthracene. This result suggests that the third electron to form the trication is incorporated into the polyacenic unit, thus supporting the experimental suggestion that the second oxidation wave corresponds to the oxidation of the polyacenic backbone. This is further confirmed by a PM3-optimization performed for $\mathbf{13a}^{3+}$, which shows that the naphthacene moiety increases its positive charge by 0.89 e in passing from $\mathbf{13a}^{2+}$ to $\mathbf{13a}^{3+}$.

Summary and Conclusions

We have synthesized a series of π-extended TTF derivatives with quinonoid structures by Wittig−Horner reaction from well-known phosphonate esters and a variety of acenequinones. The electrochemical study reveals that these compounds (**13**−**15**) exhibit good donor properties, showing a two-electron quasireversible oxidation wave to the dication and an irreversible oxidation peak to form the trication-radical. The oxidation potential values, and in a larger extent the reduction potential values in the $\text{donor}^{2+} \rightarrow \text{donor}^{0}$ process, are strongly influenced by the temperature. This behavior can be accounted for by the low stability of the cation and the high aromaticity of the dication.

The novel electron-donor molecules form CT-complexes with the strong electron-acceptor $TCNQF_4$, exhibiting a semiconducting behavior.

The molecular geometries of the unsubstituted compounds have been theoretically investigated at the semiempirical HF/PM3 and at the ab initio HF/6-31G* levels and using DFT/B3−P86/6-31G* calculations. Lateral benzoannulation determines the loss of planarity of the molecules, which adopt a butterfly-shaped structure to avoid the short contacts between the sulfur atoms and the hydrogen atoms in peri positions. The laterally fused polyacenic units always preserve their planarity and structural aromaticity. The molecular orbital distributions have been calculated using the nonempirical VEH approach. VEH calculations explain the donor properties exhibited by compounds **13**−**15** and helps to rationalize their optical properties. Lateral benzoannulation is shown to introduce new unoccupied low-energy orbitals belonging to the fused polyacenic units. For the largely extended system **15**, the HOMO → LUMO transition clearly corresponds to an electron transfer from the 1,3-dithiol-2-ylidine moieties to the laterally fused anthracene unit acting as the acceptor. The bathochromic shift observed experimentally for the largest wavelength absorption band of compounds **15** are therefore not due to a larger delocalization of the π-system, but to the appearance of an intramolecular charge-transfer band at lower energies.

The oxidation process has been studied by optimizing the molecular structures of the cations and dications. Theoretical calculations show that the gain of aromaticity is small for the cations since they remain highly distorted from planarity, preserving the butterfly structure of the neutral molecule. By contrast, the dications are fully aromatic and are constituted by a planar polyacenic unit and two singly charged dithiole rings lying orthogonal to the acene plane. The lower stability of the cation and the high aromaticity of the dication explain the coalescence of the two first oxidation potentials under the same CV wave and the temperature dependence of the reduc-

(29) Triki, S.; Ouahab. L.; Lorcy, D.; Robert, A. *Acta Crystallogr. C* **1993**, *49*, 1189.

(30) Bryce, M. R.; Coffin, M. A.; Hursthouse, M. B.; Karalouv, A. I.; Müllen, K.; Scheich, H. *Tetrahedron Lett.* **1991**, *42*, 6029.

tion peak associated to the donor^{2+} → donor^{0} process. Theoretical calculations also show that the redox properties of the dication are dominated by the polyacenic unit.

Experimental Section

1,4-Naphthacenequinone (**10**) and *n*-butyllithium (1.6 M) were commercially available. Phosphonate esters (**9a**−**c**), 6,-13-pentacenequinone (**11**), and 5,14-pentacenequinone (**12**) were obtained by previously reported procedures.[22]

Wittig−Horner Reactions. General Procedure. To a solution of phosphonate esters **9b**−**c** (1 mmol) in dry THF (20 mL) at −78 °C and under argon atmosphere was added *n*-BuLi (1.6 M) (1.1 mmol) with a syringe. After 30 min at −78 °C, the corresponding quinone, suspended in dry THF (20 mL), was added with a syringe into the solution of the phosphonate carbanion. The mixture was stirred for 1 h at −78 °C and then allowed to warm to 20 °C allowed to stand overnight. The THF was evaporated under reduced pressure, water (75 mL) added, and the residue extracted with CH_2Cl_2 (3 × 75 mL). The combined extracts were dried ($MgSO_4$) and filtered, and the solvent was removed under reduced pressure. Purification of products was achieved by column chromatography on silica gel using hexane: CH_2Cl_2 as eluent.

5,12-Bis[4,5-bis(methylthio)-1,3-dithiol-2-ylidene]-5,12-dihydronaphthacene (13b): 56% yield; mp > 250 °C; ^{1}H NMR ($CDCl_3$; 300 MHz) δ 7.88 (2H, s), 7.86 (2H, q, AA′XX′), 7.59 (2H, q, AA′XX′), 7.50 (2H, q, AA′BB′), 7.34 (2H, q, AA′XX′), 2.40 (6H, s), 2.37 (6H, s); ^{13}C NMR ($CDCl_3$; 75 MHz) δ 134.5, 138.2, 131.5, 131.4, 127.5, 126.3, 126.2, 125.8, 125.5, 125.2, 124.2, 123.5, 19.0; IR (KBr) 1600, 1530, 1495, 1455, 1420, 760 cm^{-1}; UV−vis (CH_2Cl_2) λ_{max} (log ϵ) 422 (4.50), 378 (4.44), 254 nm (4.85). Anal. Calcd for $C_{28}H_{22}S_8$: C, 54.69; H, 3.61. Found: C, 54.43; H, 3.37.

5,12-Bis(5,6-dihydro-1,3-dithiolo[4,5-*b*][1,4]dithiin-2-ylidene)-5,12-dihydronaphthacene (13c): 46% yield; mp > 250 °C; ^{1}H NMR ($CDCl_3$; 300 MHz) δ 7.92 (2H, q, AA′XX′), 7.82 (2H, s), 7.68 (2H, q, AA′XX′), 7.56 (2H, q, AA′XX′), 7.31 (2H, q, AA′XX′), 3.30 (8H, s); IR (KBr) 1600, 1530, 1500, 1450, 1440, 1290, 915, 750, 650 cm^{-1}; UV−vis (CH_2Cl_2) λ_{max} (log ϵ) 434 (3.85), 392 (3.72), 246 nm (4.23). Anal. Calcd for $C_{28}H_{18}S_8$: C, 55.05; H, 2.97. Found: C, 55.27; H, 3.18.

6,13-Bis[4,5-bis(methylthio)-1,3-dithiol-2-ylidene]-6,13-dihydropentacene (14b): 59% yield; mp > 250 °C; ^{1}H NMR ($CDCl_3$; 300 MHz) δ 7.89 (4H, s), 7.87 (4H, q, AA′XX′), 7.51 (4H, q, AA′XX′), 2.38 (12H, s); ^{13}C NMR ($CDCl_3$; 75 MHz) δ 153.7, 135.3, 133.3, 131.6, 127.5, 126.3, 125.5, 124.5, 19.1; IR (KBr) 1600, 1540, 1490, 1410, 1260, 910, 820, 800, 750 cm^{-1}; UV−vis (CH_2Cl_2) λ_{max} (log ϵ) 406 (4.35), 378 (4.34), 316 (4.35), 244 nm (4.44). Anal. Calcd for $C_{32}H_{24}S_8$: C, 57.80; H, 3.64. Found: C, 57.59; H, 3.35.

6,13-Bis(5,6-dihydro-1,3-dithiolo[4,5-*b*][1,4]dithiin-2-ylidene)-6,13-dihydropentacene (14c): 48% yield; mp > 250 °C; ^{1}H NMR ($CDCl_3$; 300 MHz) δ 7.87 (4H, q, AA′XX′), 7.85 (4H, s), 7.51 (4H, q, AA′XX′), 3.31 (8H, s); IR (KBr) 1600, 1540, 1505, 1440, 1260, 900, 810, 800, 750, 735 cm^{-1}; UV−vis (CH_2Cl_2) λ_{max} (log ϵ) 420 (3.84), 366 (4.48), 234 nm (4.27). Anal. Calcd for $C_{32}H_{20}S_8$: C, 58.15; H, 3.05. Found: C, 58.32; H, 3.19.

5,14-Bis[4,5-bis(methylthio)-1,3-dithiol-2-ylidene)-5,14-dihydropentacene (15b): 47% yield; mp > 250 °C; ^{1}H NMR ($CDCl_3$; 300 MHz) δ 8.45 (2H, s), 8.13 (2H, q, AA′BB′), 8.01 (2H, s), 7.64 (2H, q, AA′XX′), 7.50 (2H, q, AA′XX′), 7.38 (2H, q, AA′BB′), 2.44 (6H, s), 2.40 (6H, s); ^{13}C NMR ($CDCl_3$; 75 MHz) δ 135.3, 134.5, 133.3, 132.0, 131.9, 129.7, 128.0, 126.4, 125.8, 125.6, 125.5, 124.3, 123.7, 120.1, 19.0; IR (KBr) 1530, 1495, 1455, 1420, 1310, 910, 750, 650 cm^{-1}; UV−vis (CH_2Cl_2) λ_{max} (log ϵ) 460 (3.43), 388 (4.36), 268 nm (4.77). Anal. Calcd for $C_{32}H_{24}S_8$: C, 57.80; H, 3.64. Found: C, 57.59; H, 3.42.

5,14-Bis(5,6-dihydro-1,3-dithiolo[4,5-*b*][1,4] dithiin-2-ylidene)-5,14-dihydropentacene (15c): 32% yield; mp > 250 °C; ^{1}H NMR ($CDCl_3$; 300 MHz) δ 8.42 (2H, s), 8.00 (2H, q, AA′XX′), 7.92 (2H, s), 7.56 (2H, q, AA′XX′), 7.46 (2H, q, AA′XX′), 7.34 (2H, q, AA′XX′), 3.30 (8H, s); ^{13}C NMR ($CDCl_3$, 75 MHz) δ 134.5, 133.3, 132.0, 129.7, 129.0, 126.5, 125.8, 125.8, 125.8, 125.4, 124.5, 124.2, 110.7, 29.5, 29.4; IR (KBr) 1600, 1520, 1500, 1460, 1270, 915, 870, 810 cm^{-1}; UV−vis (CH_2Cl_2) λ_{max} (log ϵ) 462 (3.68), 402 (4.29), 254 nm (4.51). Anal. Calcd for $C_{32}H_{20}S_8$: C, 58.15; H, 3.05. Found: C, 57.93; H, 3.22.

Preparation of Charge-Transfer Complexes. General Procedure. To a boiling solution of the corresponding donor (**13**, **14b**−**c**) (0.1 mmol) in dry CH_2Cl_2 (10 mL) under argon atmosphere was added a solution of $TCNQF_4$ (0.4 mmol). The resultant dark blue solution was refluxed for 30 min, and the mixture was slowly cooled to 0 °C. The solid precipitated was collected by filtration, washed with cold CH_2Cl_2 (3 × 5 mL), and dried in vacuo to give the corresponding complex.

Complex 5,12-bis[4,5-bis(methylthio)-1,3-dithiol-2-ylidene]-5,12-dihydronaphthacene (13b)−$TCNQF_4$ (1:2: 1CH_2Cl_2 stoichiometry): 34% yield; mp > 250 °C; FT-IR (KBr) 2193, 2174, 1541, 1518, 1382, 1338, 1315, 1213, 983, 864 cm^{-1}; UV−vis (MeCN) λ_{max} 855, 752, 685, 413, 347, 278, 234 nm. Anal. Calcd for $C_{53}H_{24}F_8N_8Cl_2$: C, 50.84; H, 1.93; N, 8.95. Found: C, 51.01; H, 2.13; N, 8.79.

Complex 5,12-bis(5,6-dihydro-1,3-dithiolo[4,5-*b*][1,4]dithiin-2-ylidene)-5,12-dihydronaphthacene (13c)−TCNQF$_4$ (1:2:0.5 CH_2Cl_2 stoichiometry): 41% yield; mp > 250 °C; FT-IR (KBr) 2196, 2174, 1536, 1512, 1396, 1338, 1319, 1203, 981 cm^{-1}; UV−vis (MeCN) λ_{max} 855, 752, 686, 405, 234 nm. Anal. Calcd for $C_{105}H_{38}F_{16}N_{16}S_{16}Cl_2$: C, 52.30; H, 1.59; N, 9.25. Found: C, 52.21; H, 1.58; N, 9.35.

Complex 6,13-bis[4,5-bis(methylthio)-2-ylidene]-6,13-dihydropentacene (14b)−$TCNQF_4$ (1:2:0.5 CH_2Cl_2 stoichiometry): 36% yield; mp > 250 °C; FT-IR (KBr) 2192, 2174, 1534, 1497, 1408, 1388, 1347, 1338, 1323, 1201, 1142, 968 cm^{-1}; UV−vis (MeCN) λ_{max} 683, 753, 855, 362, 289, 245 nm. Anal. Calcd for $C_{113}H_{50}F_{16}N_{16}S_{16}Cl_2$: C, 53.87; H, 2.00; N; 8.89. Found: C, 53.60; H, 1.81; N, 8.49.

Complex 6,13-bis(5,6-dihydro-1,3-dithiolo[4,5-*b*][1,4]dithiin-2-ylidene)-6,13-dihydropentacene (14c)−$TCNQF_4$ (1:2:2 CH_2Cl_2 stoichiometry): 38% yield; mp > 250 °C; FT-IR (KBr) 2197, 2174, 1537, 1499, 1403, 1390, 1348, 1338, 1292, 1265, 1200, 1144, 1072, 1052, 969, 888, 876, 741 cm^{-1}; UV−vis (MeCN) λ_{max} 855, 753, 684, 394, 262 nm. Anal. Calcd for $C_{58}H_{24}N_8F_8S_8Cl_4$: C, 50.37; H, 1.75; N, 8.10. Found: C, 50.81; H, 1.58; N, 8.18.

Computational Methods

Calculations were performed on IBM RS/6000 workstations and on a SGI Power Challenge L R8000 computer at the Departamento de Química Física of the University of Valencia. Geometry optimizations were carried out at the HF level using both the semiempirical PM3 method,[31] as implemented in the MOPAC 6.0 program,[32] and standard ab initio calculations using the split-valence, double-ζ, polarized 6-31G* basis set[33] and the GAUSSIAN 94 program.[34] Additional calculations were done at the density functional theory (DFT) level using the hybrid gradient corrected B3−P86 density functional[35] and the 6-31G* basis set.

The geometries of neutral molecules and dications were computed within the restricted Hartree−Fock (RHF) for-

(31) Stewart, J. J. P. *J. Comput. Chem.* **1989**, *10*, 209; **1989**, *10*, 221.

(32) Stewart, J. J. P. MOPAC: A General Molecular Orbital Package (version 6.0); QCPE, **1990**, *10*, 455.

(33) Hariharan, P. C.; Pople, J. A. *Chem. Phys. Lett.* **1972**, *16*, 217.

(34) Frisch, M. J.; Trucks, G. W.; Schlegel, H. B.; Gil, P. M. W.; Johnson, B. G.; Robb, M. A.; Cheeseman, J. R.; Keith, T.; Petersson, G. A.; Montgomery, J. A.; Raghavachari, K.; Al-Laham, M. A.; Zakrzewski, V. G.; Ortiz, J. V.; Foresman, J. B.; Cioslowski, J.; Stefanov, B. B.; Nanayakkara, A.; Challacombe, M.; Peng, C. Y.; Ayala, P. Y.; Chen, W.; Wong, M. W.; Andres, J. L.; Replogle, E. S.; Gomperts, R.; Martin, R. L.; Fox, D. J.; Binkley, J. S.; Defrees, D. J.; Baker, J.; Stewart, J. P.; Head-Gordon, M.; Gonzalez, C.; Pople, J. A. Gaussian 94, Revision B.1, Gaussian Inc.: Pittsburgh, PA, 1995.

(35) Perdew, J. P. *Phys. Rev. B* **1986**, *33*, 8822.

malism, while the spin-unrestricted Hartree−Fock (UHF)[36] approximation, where electrons with different spins occupy different sets of orbitals, was used for singly charged cations. In all the PM3 calculations, the gradient norm achieved was lower than 0.05. For ab initio and DFT calculations, the Berny analytical gradient method[37] was used for the optimizations and the threshold values for the maximum force and the maximum displacement were 0.00045 and 0.0018 atomic units, respectively.

The electronic structure was investigated using the nonempirical valence effective Hamiltonian (VEH) pseudopotential technique.[38] This technique takes only into account the valence electrons and is based on the use of an effective Fock Hamiltonian where all the parameters used to build up the atomic potentials are optimized to reproduce the results of ab initio Hartree−Fock calculations. The VEH method is thus completely nonempirical since no experimental data enter the effective Fock Hamiltonian. It constitutes an especially useful tool to deal with large molecular systems, since it yields one-electron energies of ab initio double-ζ quality without performing any self-consistent-field (SCF) process or calculating any bielectronic integral. All the VEH calculations were performed using the atomic potentials previously optimized for hydrogen, carbon and sulfur atoms.[39] The validity of the VEH approach to study the electronic structure of large π-electronic molecular systems has been widely illustrated.[28,40,41]

Acknowledgment. The groups at Madrid and Valencia jointly acknowledge financial support by the CICYT Grant No. PB95-0428-CO2. One of the authors (L.S.) is indebted to M.E.C. for a research fellowship.

JO9719416

(36) Pople, J. A.; Nesbet, R. K. *J. Chem. Phys.* **1954**, *22*, 571.
(37) Schlegel, H. B. *J. Comput. Chem.* **1982**, *3*, 214.

(38) Nicolas, G.; Durand, Ph. *J. Chem. Phys.* **1979**, *70*, 2020; **1980**, *72*, 453. André, J. M.; Burke, L. A.; Delhalle, J.; Nicolas, G.; Durand, Ph. *Int. J. Quantum Chem. Symp.* **1979**, *13*, 283. Brédas, J. L.; Chance, R. R.; Silbey, R.; Nicolas, G.; Durand, Ph. *J. Chem. Phys.* **1981**, *75*, 255.

(39) (a) André, J. M.; Brédas, J. L.; Delhalle, J.; Vanderveken, D. J.; Vercauteren, D. P.; Fripiat, J. G. In *Modern Techniques in Computational Chemistry: MOTECC-90*; Clementi, E., Ed.; Escom: Leiden, The Netherlands, 1990; p 745. (b) Brédas, J. L.; Thémans, B.; André, J. M. *J. Chem. Phys.* **1983**, *78*, 6137.

(40) Ortí, E.; Brédas, J. L. *J. Chem. Phys.* **1998**, *89*, 1009. Ortí, E.; Brédas, J. L. *Chem. Phys. Lett.* **1989**, *164*, 247. Ortí, E.; Brédas, J. L.; Clarisse, C. J. *Chem. Phys.* **1990**, *92*, 1228. Ortí, E.; Piqueras, M. C.; Crespo, R.; Brédas, J. L. *Chem. Mater.* **1990**, *2*, 110.

(41) Bando, P.; Martín, N.; Segura, J. L.; Seoane, C.; Ortí, E.; Viruela, P. M.; Viruela, R.; Albert, A.; Cano, F. H. *J. Org. Chem.* **1994**, *59*, 4618.